Techniques for Measuring Phase Closure at 11 Microns

David D. S. Hale, W. Fitelson, J. D. Monnier[a], J. Weiner, and C. H. Townes

ISI Array at Space Sciences Laboratory
University of California at Berkeley
Berkeley, CA, 94720-7450, USA

[a]Harvard-Smithsonian Center for Astrophysics, Cambridge, MA, USA

ABSTRACT

The U.C. Berkeley Infrared Spatial Interferometer (ISI), previously described by Hale et al.[1] as a two-telescope stellar interferometer operating in the mid-infrared regime of 9–12 μm, is now testing a recently constructed third telescope and centralized laser local oscillator and beam combining facilities for operation of a three-telescope system with phase closure. This new system will allow the ISI Array to make measurements of stellar photospheric and dust asymmetries in the mid-IR, measurements which have previously been lacking. The new facilities and instrumentation required for three-way heterodyne beam combination and fringe detection, together with techniques for measuring the closure phase, are described. Both hardware and software methods of beam combination are used for producing three simultaneous fringe visibilities and a closure phase measurement. Additionally, the phase closure signal-to-noise of pairwise and of all-in-one beam combination are contrasted.

Keywords: Instrumentation, Closure Phase, Infrared, Interferometry

1. INTRODUCTION

The ISI Array consists of three 1.65m movable telescopes with possible separations currently ranging from 4m to about 70m, and an adjustable operating wavelength range of 9–12μm. Although the two-element ISI was described fairly recently,[1] a brief summary is given here to provide context for the descriptions of the new three-element system and phase closure methods.

Heterodyne detection is utilized at each of the three ISI apertures, a scheme which involves the use of a CO_2 laser local oscillator (LO) inside each telescope for the purpose of downconverting the frequency of the received mid-infrared stellar radiation. The CO_2 laser LO in each telescope is spatially mixed with the stellar signal collected by that telescope's aperture onto a HgCdTe photodiode. Of the resultant sum and difference frequencies produced by this mixing process, only the difference between the stellar and laser radiation frequencies is within the bandwidth of the detector, and it is that which forms what is known as the *intermediate frequency*, or IF signal. The IF bandpass for the ISI is in the radio frequency (RF) regime and currently extends from 200 to 2800 MHz, providing a double sideband (DSB) bandwidth of approximately $5\frac{1}{2}$ GHz. After heterodyne detection of the mid-IR stellar signal, all of the subsequent steps required for interferometry are performed at radio frequencies using the IF signals. The IF can be split, amplified and routed to a number of different locations for a variety of different purposes without loss of signal or additional degradation of signal to noise ratio (S/N). This is one of the benefits of using heterodyne over direct detection. (A more detailed comparison between heterodyne and direct detection has been made elsewhere.[1])

In order to meaningfully correlate the IF signals from two or more telescopes for the purpose of measuring interference fringes, the phase relationship between each telescope's laser local oscillator must be fixed, or at least well known. We create a fixed phase relationship between each of the telescope lasers. In the new three-telescope array, this is accomplished by the introduction of a centralized Master Laser Local Oscillator Facility

Further author information: (Send correspondence to D.D.S.H.)
D.D.S.H.: E-mail: david@isi.mtwilson.edu, Address: Mount Wilson Observatory, Mount Wilson, CA, 91023, USA

(MLOF) which houses a laser similar to those contained in the telescopes. This "master" laser is split into three beams which are sent through open air paths to each telescope. Multiple feedback loops are then used to lock the frequency and phase of the telescope lasers onto the master laser, and to compensate for pathlength variations between the MLOF and the telescopes. The pathlengths traveled by the master laser between the MLOF and the three telescopes are each actively controlled to a precision of approximately $\frac{\lambda}{100}$ (where $\lambda \approx 11\mu$m) at a rate of ~ 20 Hz, and the phase relationship of all lasers is held to within $\pm 5°$.

As a star moves across the sky due to diurnal motion, the geometrical delay of a stellar wavefront which reaches the various interferometer elements is continually changing, an effect which is removed in the standard way by introducing a variable delay line. However, since the delay is inserted at the heterodyne IF stage, the stellar signals traverse the geometrical delay and the delay line at different frequencies, resulting in a differential Doppler shift between the signals from each telescope. This causes a modulation of the fringes at what is called the *natural fringe frequency*. The ISI Array performs what is known in radio astronomy as *lobe rotation*, whereby we eliminate the natural fringe frequency modulation by adjusting the relative phases of the local oscillators. The lobe rotator, or *phase shifter*, serves an additional purpose as well, which will be described in section 2.1.

2. BEAM COMBINATION

Beam combination and fringe production are performed at radio frequencies by using the heterodyne IF signals discussed in section 1. Figure 1 shows a schematic representation of the ISI, with emphasis placed upon the signal paths leading to fringe production.

After heterodyne detection of the stellar radiation collected at each telescope, the IF signals are carried over coaxial cables into a central control room facility (a nearby building which is separate from the telescopes, where an observer also operates and monitors all of the various functions of the ISI Array). It is here that the effects of the difference in geometrical delay of the light between the three interferometer elements are removed by appropriately delaying two of the IF signals. Each delay line consists of a bank of binary ordered lengths (i.e. 1 cm, 2 cm, 4 cm, etc.) of coaxial cables which are switched into place using computer-controlled RF relays, in increments which allow us to track the *white light* fringe.

2.1. Lobe Rotator and Fringe Detection

The *lobe rotators*, or phase shifters, are indicated in figure 1 by the blocks labeled ϕj and serve to induce phase shifts ϕ_{LO_j} on the local oscillator of telescope j. As is standard practice in radio astronomy the lobe rotators are used to continually vary the phases of the local oscillators which in turn cancels out the effects of natural fringe frequency modulation ($\nu_{\mathrm{NFF}_{jk}}$) on the fringe products taken between a pair of interferometer elements j and k. Secondly, the lobe rotators are used to introduce a fixed ($\nu_{\mathrm{PLL}} \equiv +1\,\mathrm{MHz}$) frequency offset of each telescope's laser with respect to the master laser. This offset provides a reference and an error signal upon which the phase lock loop (PLL) feedback system operates. Since each LO is given this same offset with respect to the master laser, the effect of adding it will cancel out in the fringe signal. After introducing $\nu_{\mathrm{PLL}} + \nu_{\mathrm{NFF}_{jk}}$ and appropriately matching the phase of each telescope's IF signal by means of the delay lines, the IF signals between any pair of telescopes can, in principle, be correlated to produce fringes. However, in doing so the fringe signals would be static, that is, at zero frequency. Since from an instrumentation point of view it is difficult to measure low-level DC signals, we use the lobe rotators to add additional offsets (ν_{F_j}) to each local oscillator in such a way that the fringe signal produced by each pair of baselines emerges at a given unique and constant frequency. Thus, the lobe rotator phase for telescope j's local oscillator is the sum of these three phase adjustments, or

$$\phi_{\mathrm{LO}_j} = (\nu_{\mathrm{PLL}} + \nu^j_{\mathrm{NFF}} + \nu_{F_j})t\,, \tag{1}$$

where

$$\nu_{\mathrm{PLL}} \equiv 1\,\mathrm{MHz} \tag{2a}$$

$$\nu^j_{\mathrm{NFF}} = 0,\ \nu_{\mathrm{NFF}_{12}},\ \nu_{\mathrm{NFF}_{31}} \tag{2b}$$

$$\nu_{F_j} = 166,\ 93,\ 0\ \mathrm{Hz} \tag{2c}$$

are the PLL offset frequency (2a), the natural fringe frequency corrections (2b), and the induced fringe offset frequencies (2c) for telescopes $j = 1, 2, 3$, respectively.

The delayed and phase compensated IF "beams" are multiplied together in pairs using RF correlators, producing three fringe signals ($F_{\vec{jk}}$), one for each pair of baselines between telescopes j and k. Our RF correlators are represented in detail in figure 1 by the collection of hybrid, RF detector diodes and differential amplifier. The phases of the three fringe pairs produced by the correlators for the Tel $\vec{12}$, Tel $\vec{23}$, and Tel $\vec{31}$ baselines can be expressed as

$$\Phi_{F_{\vec{jk}}} = \phi_{\mathcal{V}_{jk}} + [\varphi_k(t) - \varphi_j(t)] - \nu_{\mathrm{NFF}_{jk}} t + [\phi_{\mathrm{LO}_j} - \phi_{\mathrm{LO}_k}] \,, \tag{3}$$

where we introduce here the terms $\varphi_j(t)$, which represent atmospheric fluctuations above telescope j, and $\phi_{\mathcal{V}_{jk}}$, which are the complex Fourier components of the visibility for the fringe pair between telescopes j and k. Substituting equations (1) and (2) into equation (3), results in

$$\Phi_{F_{\vec{12}}} = \phi_{\mathcal{V}_{12}} + [\varphi_2(t) - \varphi_1(t)] + (2\pi\ 73\,\mathrm{Hz})t \,, \tag{4a}$$

$$\Phi_{F_{\vec{23}}} = \phi_{\mathcal{V}_{23}} + [\varphi_3(t) - \varphi_2(t)] + (2\pi\ 93\,\mathrm{Hz})t \,, \text{and} \tag{4b}$$

$$\Phi_{F_{\vec{31}}} = \phi_{\mathcal{V}_{31}} + [\varphi_1(t) - \varphi_3(t)] - (2\pi 166\,\mathrm{Hz})t \,, \tag{4c}$$

where we now see one result of the frequency selection in equation (2c), which is to produce fringes with an audio frequency modulation. The frequencies of equation (2c) were selected in part to modulate the fringes at frequencies that are both relatively far apart from each other and from 60 Hz and its harmonics. They were also selected such that the maximum frequency is well below the Nyquist frequency (250 Hz) in order to allow ample room for analog filtering which will prevent aliasing noise. Further relevance of these particular frequencies will be shown in section 3.

The audio fringe frequencies produced by the correlators are digitized by a fast (500 Hz) analog to digital converter (FADC), and recorded onto computer disk. Determination of the fringe power for each of the three baseline pairs is a relatively simple matter of calculating the Fourier transform of each digitized signal and looking at the power within some bandwidth centered about these three frequencies. This will be discussed in more detail in section 3. Note that only the three fringe *pairs* are interfered in hardware; other processing is done by computation. An all-in-one triple product of fringe signals could alternatively be produced entirely by hardware, but this appears less advantages than flexible computational processing.

3. BISPECTRUM MEASUREMENT

The situation described so far is the exact same method that has been successfully used since 1988 for the ISI as a two-element interferometer, and the development of a three-element interferometer merely required the duplication of existing and proven hardware (e.g. correlator, delay line, lobe rotator, and optical systems such as PLL and PLC). This approach of duplicating existing systems, as opposed to developing and troubleshooting new, very fast hardware for a three-way IF "beam" combiner somewhat influenced the decision to interfere only pairs of signals in hardware, and to perform the remaining steps for obtaining the triple product (and closure phase) in software.

Using the fringe phases expressed in equation (4), we can write a simplified form of the three correlated fringe signals $F_{\vec{jk}}$ recorded by the FADC as

$$F_{\vec{12}}(t) \propto \sqrt{2P_{12}} \cos \Phi_{F_{\vec{12}}} = \sqrt{2P_{12}} \left[\tfrac{1}{2} e^{i\left(2\pi\ 73t + \phi_{\mathcal{V}_{12}} + \varphi_2(t) - \varphi_1(t) \right)} + \tfrac{1}{2} e^{i\left(-2\pi\ 73t - \phi_{\mathcal{V}_{12}} - \varphi_2(t) + \varphi_1(t) \right)} \right] + q_{\vec{12}} \tag{5a}$$

$$F_{\vec{23}}(t) \propto \sqrt{2P_{23}} \cos \Phi_{F_{\vec{23}}} = \sqrt{2P_{23}} \left[\tfrac{1}{2} e^{i\left(2\pi\ 93t + \phi_{\mathcal{V}_{23}} + \varphi_3(t) - \varphi_2(t) \right)} + \tfrac{1}{2} e^{i\left(-2\pi\ 93t - \phi_{\mathcal{V}_{23}} - \varphi_3(t) + \varphi_2(t) \right)} \right] + q_{\vec{23}} \tag{5b}$$

$$F_{\vec{31}}(t) \propto \sqrt{2P_{31}} \cos \Phi_{F_{\vec{31}}} = \sqrt{2P_{31}} \left[\tfrac{1}{2} e^{i\left(-2\pi 166t + \phi_{\mathcal{V}_{31}} + \varphi_1(t) - \varphi_3(t) \right)} + \tfrac{1}{2} e^{i\left(2\pi 166t - \phi_{\mathcal{V}_{31}} - \varphi_1(t) + \varphi_3(t) \right)} \right] + q_{\vec{31}} \tag{5c}$$

where P_{jk} represents the power in the fringe between interferometer elements j and k, and we include here a term $q_{\vec{jk}}$ which represents the intrinsic quantum noise associated with the detection process, as well as any other unidentified source of random noise.

To measure the bispectrum we first apply software filters to each of the above recorded signals $F_{\vec{12}}$, $F_{\vec{23}}$, and $F_{\vec{31}}$, which are centered about the frequencies 73 Hz, 93 Hz, and -166 Hz, respectively. The bandwidth of the filters is dependent upon the level of atmospheric turbulence (i.e. "seeing") and, although variable from one observation to the next, is typically 5 Hz wide. (Sometimes this will be less for excellent seeing, and sometimes will be as wide as 10 Hz for poor seeing conditions.) Note that these are only example values; any fringe bandwidth filter can be chosen to optimize S/N, and the importance of this is shown in section 4.

At this point we can employ a fairly common method for measuring the bispectrum. This involves breaking up the data into small chunks of length equal to the coherence time and determining the bispectral components within those coherent bins. In our case we may estimate the average coherence time over an integration by a measure of the width of the fringes in frequency space (see figure 2). The fringe width $\delta\nu_F$ is identified from the power spectrum of equation (5) and the coherence time as $t_c \approx \frac{1}{\delta\nu_F}$. We then calculate the Fourier transform within each of these small coherent bins which have been defined by a Hanning window, and form a bispectrum datum within each coherent bin from the product of the three windowed Fourier transforms. A mean bispectrum is obtained from the average of all of the coherently binned bispectra. In other words,

$$\langle \text{bispectrum} \rangle = \frac{1}{N_{\delta\nu_F}} \sum_i \text{FFT}_{\nu_{12}} \left[F_{\vec{12}}(t_i + t_c) H(t_c) \right] \cdot \text{FFT}_{\nu_{23}} \left[F_{\vec{23}}(t_i + t_c) H(t_c) \right] \cdot \text{FFT}_{\nu_{31}} \left[F_{\vec{31}}(t_i + t_c) H(t_c) \right] , \tag{6}$$

where $\text{FFT}_{\nu_{jk}}$ denotes the Fast Fourier Transform evaluated only at the single frequency component identified by the fringe frequency ν_{jk} between interferometer elements j and k, the summation is done over the entire data set in steps of the fringe width $\delta\nu_F$, $N_{\delta\nu_F}$ denotes the number of coherent bins of size $\delta\nu_F$, t_c is the coherence time, and $H(t_c)$ denotes a Hanning window function of width equal to the coherence time, t_c.

An equivalent and computationally somewhat more streamlined method is to form the bispectrum product over the entire length of the integration, rather than within small coherent bins. Multiplying together all three filtered fringe signals of equation (5) we form the bispectrum,

$$F_{123}(t) = F_{\vec{12}} \cdot F_{\vec{23}} \cdot F_{\vec{31}} = \frac{1}{2} \sqrt{\frac{P_{12} P_{23} P_{31}}{2}} \, e^{i\left(2\pi 0 t + \phi_{\nu_{12}} + \phi_{\nu_{23}} + \phi_{\nu_{31}}\right)} + \mathcal{N}_{\delta\nu_0} , \tag{7}$$

where $\mathcal{N}_{\delta\nu_0}$ represents all of the cross terms containing noise within the filter bandwidth now centered around zero frequency. We see that the random atmospheric phase fluctuations $\varphi_j(t)$ have cancelled themselves completely, leaving only the sum of the original Fourier phases which are intrinsic to the unperturbed fringe signals. The magnitude and phase (i.e. the closure phase) of the triple product are then,

$$|\mathcal{V}_{123}| = \frac{1}{2} \sqrt{\frac{P_{12} P_{23} P_{31}}{2}} , \qquad \text{and} \tag{8a}$$

$$\Phi_{\text{CL}} = \phi_{\mathcal{V}_{12}} + \phi_{\mathcal{V}_{23}} + \phi_{\mathcal{V}_{31}} = \arctan \left[\frac{\langle \text{Im}\, F_{123} \rangle}{\langle \text{Re}\, F_{123} \rangle} \right] , \tag{8b}$$

where $\langle F_{123} \rangle$ is simply the complex average of equation (7). The width of the triple fringe will be inversely proportional to the integration time, and is limited only by the width of the discrete Fourier transform components. Therefore the only noise on this signal is that which falls within the single FFT pixel. This is not negligible, because multiplication of the three fringes allows a beat frequency of zero between a wide range of noise frequencies, as well as beats between signals and noise.

3.1. Precision of Measurements

The expected quality of the S/N can be estimated by considering the $\mathcal{N}_{\delta\nu_0}$ term of equation (7). This term consists of three cross terms involving noise of the form, $n^3 + n^2\, s + n\, s^2$, where n refers to noise and s refers to signal terms. The result can be compared with the signal to noise of a fringe signal.

For an average over a bandwidth $\delta\nu$ containing a fringe, the signal to noise ratio for the power in an individual fringe is

$$\left(\frac{S}{N}\right)_{\mathrm{F}} = \frac{P}{\sigma_q^2}\frac{\sqrt{T\delta\nu}}{\sqrt{1+2\frac{P}{\sigma_q^2}}}\,, \tag{9}$$

where P is the average power per unit bandwidth of a fringe, σ_q^2 the noise power per unit bandwidth, and T the total time of averaging. For the phase closure product of the three fringes, each of which having the same signal to noise, the corresponding signal to noise ratio for the triple amplitude or for closure phase is[2]

$$\left(\frac{S}{N}\right)_{\mathrm{tp}} = \left(\frac{P}{\sigma_q^2}\right)^{\frac{3}{2}}\frac{\sqrt{2T\delta\nu}}{\sqrt{3\left(\frac{P^2}{\sigma_q^4}+\frac{P}{\sigma_q^2}+\frac{1}{4}\right)}}\,. \tag{10}$$

When the signal to noise in one coherence time is much less than 1, that is, if $(S/N)_{t_c} \equiv P/\sigma_q^2 \ll 1$, then

$$\left(\frac{S}{N}\right)_{\mathrm{F}} = \frac{P}{\sigma_q^2}\sqrt{T\delta\nu}\,, \tag{11a}$$

and

$$\begin{aligned}\left(\frac{S}{N}\right)_{\mathrm{tp}} &= \sqrt{\frac{8}{3}}\left(\frac{P}{\sigma_q^2}\right)^{\frac{3}{2}}\sqrt{T\delta\nu}\\ &= \sqrt{\frac{8}{3}}\,(T\delta\nu)^{-\frac{1}{4}}\left(\frac{S}{N}\right)_{\mathrm{F}}^{\frac{3}{2}}\\ &= \sqrt{\frac{8}{3}\frac{P}{\sigma_q^2}}\left(\frac{S}{N}\right)_{\mathrm{F}}\,.\end{aligned} \tag{11b}$$

When the signal to noise in one coherence time $(S/N)_{t_c} \gg 1$, then

$$\left(\frac{S}{N}\right)_{\mathrm{F}} = \sqrt{\frac{P}{2\sigma_q^2}T\delta\nu}\,, \tag{12a}$$

and

$$\begin{aligned}\left(\frac{S}{N}\right)_{\mathrm{tp}} &= \left(\frac{P}{\sigma_q^2}\right)^{\frac{1}{2}}\sqrt{\frac{2T\delta\nu}{3}}\\ &= \frac{2}{\sqrt{3}}\left(\frac{S}{N}\right)_{\mathrm{F}}\,.\end{aligned} \tag{12b}$$

A typical fringe measurement with the two-element ISI would have a fringe bandwidth $\delta\nu \approx 5\,\mathrm{Hz}$ and an integration time $T = 4$ minutes, so that equation (11a) would give a single fringe power signal to noise ratio $(S/N)_{\mathrm{F}} \approx 35\frac{P}{\sigma_q^2}$. Thus characteristically $(S/N)_{t_c} \ll 1$ even when the average $(S/N)_{\mathrm{F}}$ of a fringe is relatively large (~ 35), and equation (11b) is a good approximation for all but a handful of the brightest stars observable with the ISI. Equation (12b) shows that even in the few cases where $(S/N)_{t_c}$ is very high, then the signal to noise ratio for the closure phase cannot be much larger than the signal to noise ratio for power in a single fringe.

The value of $(S/N)_{\mathrm{tp}}$ can be optimized by using a fringe bandwidth $\delta\nu$ somewhat narrower than that needed for an optimum measurement of the fringe power. This is because the fringe signal peaks at the fringe frequency and decreases over the bandwidth whereas the noise power is uniform over the bandwidth. Consider,

for example, a fringe power distribution which is Gaussian in shape with a $\frac{1}{e}$ width of $\delta\nu_e$. In order to not lose more than 1% of the power, a bandwidth at least as large as about $1.9\delta\nu_e$ is required. In the high $(S/N)_{t_c}$ case of equation (12b), $(S/N)_{\rm tp}$ is maximized when $\delta\nu \approx \delta\nu_e$, for which $(S/N)_{\rm F}$ is larger by a factor of approximately 1.27. For the low $(S/N)_{t_c}$ case of equation (11b), the phase signal to noise is improved over the fringe signal to noise by a factor of approximately 1.7. Hence it can be advantageous to calculate the phase closure with a narrower bandwidth per fringe than that used for an accurate visibility determination.

As an example of likely precision obtainable, on a relatively long 56m baseline the two element ISI might reasonably detect fringes with a S/N ≈ 15 after a 4 minute integration time and a 5 Hz fringe bandwidth (see top panel in figure 2). This implies, from equation (11b), a phase error of approximately 3.6°. Shorter baselines and longer integrations should provide still higher precision.

4. PHASE CLOSURE SIMULATIONS

The potential results obtainable with these two methods can be illustrated by a series of simulations based upon the representation of the fringe signals given by equation (5). We model the noise with a random distribution having a noise power per unit frequency of σ_q^2. The atmospheric phase fluctuations, $\varphi_j(t)$ are modeled according to Kolmogorov theory*, giving a power spectrum which is proportional to $\sigma_p^2 \cdot \text{frequency}^{-8/3}$ where σ_p is a constant used to describe the distribution of the phase fluctuations and is determined empirically to match observed conditions with the two-telescope ISI. With these assumptions and equation (5) we generate a series of simulated fringe signals, one of which is compared to an actual two-element ISI fringe in figure 2. We then compute the bispectrum using this simulated data which has a known input closure phase. The results of determining this closure phase using the methods described in section 3 are shown in figure 3. The figure shows a measured error in the closure phase of approximately 3°, which is in reasonable agreement with the predictions made in section 3.1. Figure 3 also indicates an optimum bandwidth for which we maximize the S/N. The occurrence of this minimum at approximately 3 Hz might be reasonably expected from the width of the fringes used in the simulations, which can be seen in figure 2. Note the narrower optimum bandwidth of 3 Hz for the phase measurement, which does not fully enclose all of the fringe power, while the optimum bandwidth for accurate visibility measurement is approximately 5 Hz. As a further check of the assumptions made in sections 3.1, a set of simulated fringes was produced with high enough noise such that $(S/N)_{t_c} \ll 1$, that is, the S/N in one coherence time was much less than 1. These simulated fringes were measured for various times of integration to improve the S/N. The measured ratios between S/N in a single fringe and the triple product are shown in figure 4, along with the prediction given by equation (11b).

5. SUMMARY

The ISI has recently been upgraded with the addition of a third telescope and centralized laser local oscillator and heterodyne beam combining facilities. When fully completed, it will be able to measure three simultaneous visibility values and phase closure in the 9–12 μm wavelength regime. The new ISI Array will record three separate fringe signals which have been modulated at audio frequencies and digitized, providing some flexibility in determinating the bispectrum components through modifiable computer software programs. We have examined two possible techniques which can be used for analyzing the new data, and have compared favorably the expected quality of the actual measurements against simulated data. The expected error in the phase closure should be a few degrees or less for typically good fringe signals.

ACKNOWLEDGMENTS

This work was supported by grants from the National Science Foundation, the Office of Naval Research, and the Gordon & Betty Moore Foundation.

*While the details of the timescale and structure function of this theory may not be precise as applied here, it is not essential that the exact nature of atmospheric fluctuations be duplicated for the purpose of this particular simulation application.

REFERENCES

1. D. D. S. Hale, M. Bester, W. C. Danchi, W. Fitelson, S. Hoss, E. A. Lipman, J. D. Monnier, P. G. Tuthill, and C. H. Townes, "The Berkeley Infrared Spatial Interferometer: A heterodyne stellar interferometer for the mid-infrared," *Astrophysical Journal* **537**, pp. 998–1012, 2000.
2. T. J. Cornwell, "Radio-interferometric imaging of weak objects in conditions of poor phase stability: the relationship between speckle masking and phase closure methods," *Astronomy & Astrophysics* **180**, pp. 269–274, 1987.

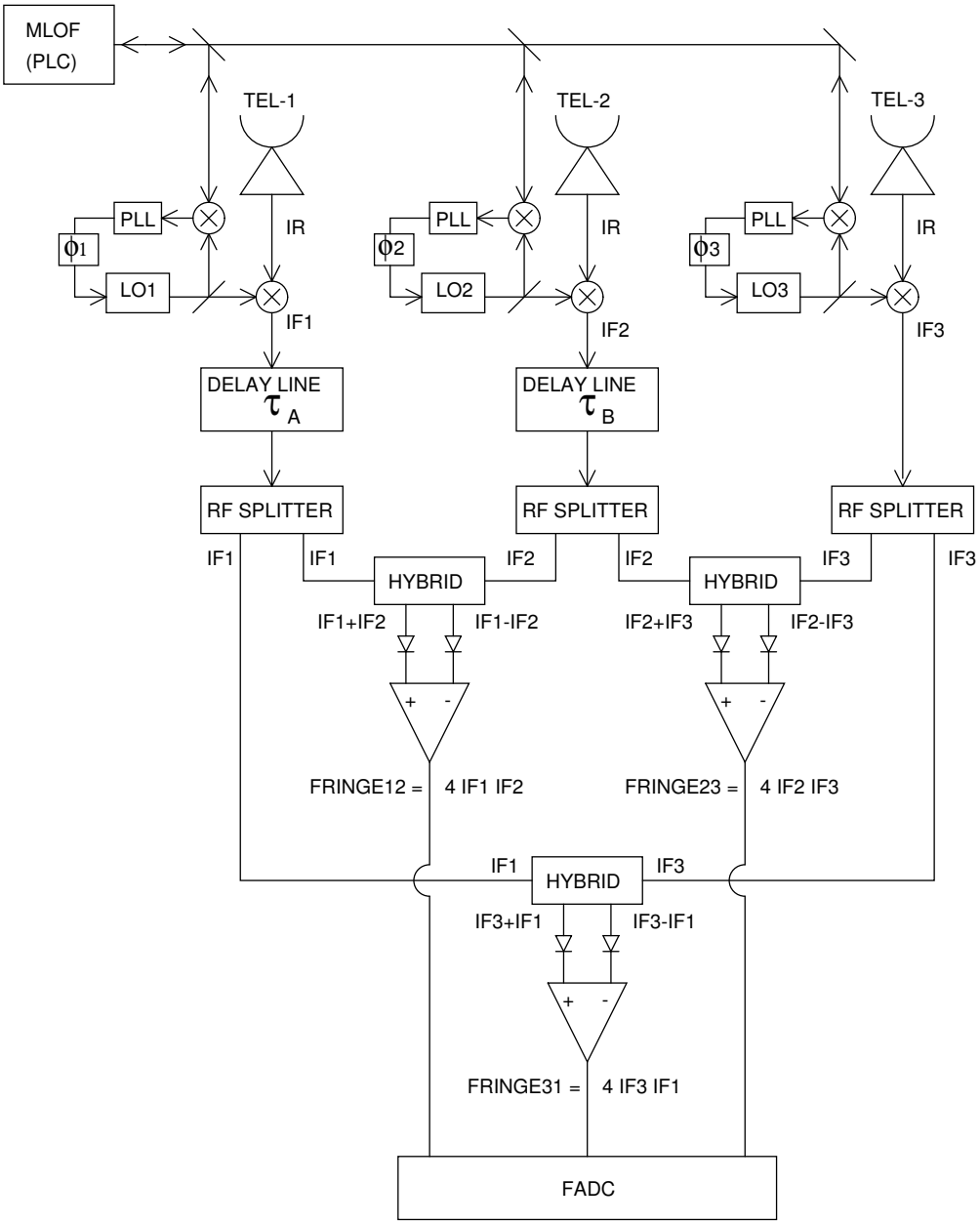

Figure 1. Schematic diagram of ISI signal paths. Infrared (IR) radiation from a star is mixed onto a detector with radiation from an IR laser local oscillator (LOj), which produces a radiofrequency IFj signal. The phase of each LOj is fixed with respect to a "master" laser by means of a phase lock loop (PLL). The PLL system includes the ability to input phase shifts onto each LOj (indicated by blocks labeled ϕj). This serves as the lobe rotator, and additionally gives us the ability to sweep each fringe pair at a different frequency. The box labeled "HYBRID" is a device whose two outputs are equal to the vector sum and difference of the two inputs. A hybrid, two RF detector diodes, and a differential amplifier combined form a correlator. FADC is the Fast Analog to Digital Converter which digitally samples the fringes and stores them on a computer disk for processing.

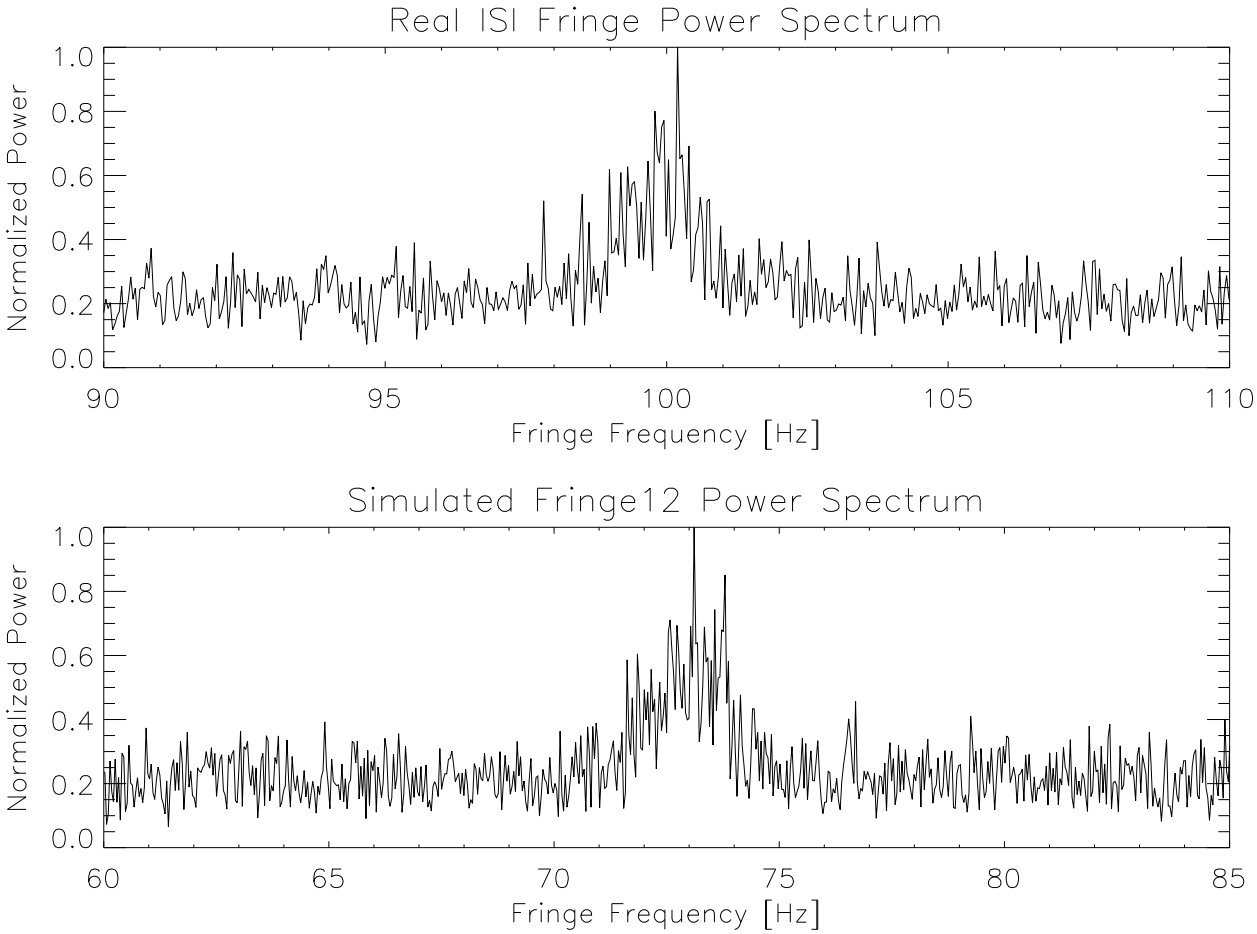

Figure 2. ISI Fringe Power Spectra. The top panel is a real fringe recorded by the two-telescope ISI on 19Dec01 for o Ceti with a 56m baseline. The bottom panel shows a sample simulated fringe (for the Tel $\vec{1}\vec{2}$ baseline) generated by equation (5a). Simulated fringes such as this were generated for each of the three baseline pairs and were then used in computing the bispectrum. Both data sets above represent a four minute integration time, and are plotted with $\frac{1}{24}$ second binning (i.e. 10 points/average).

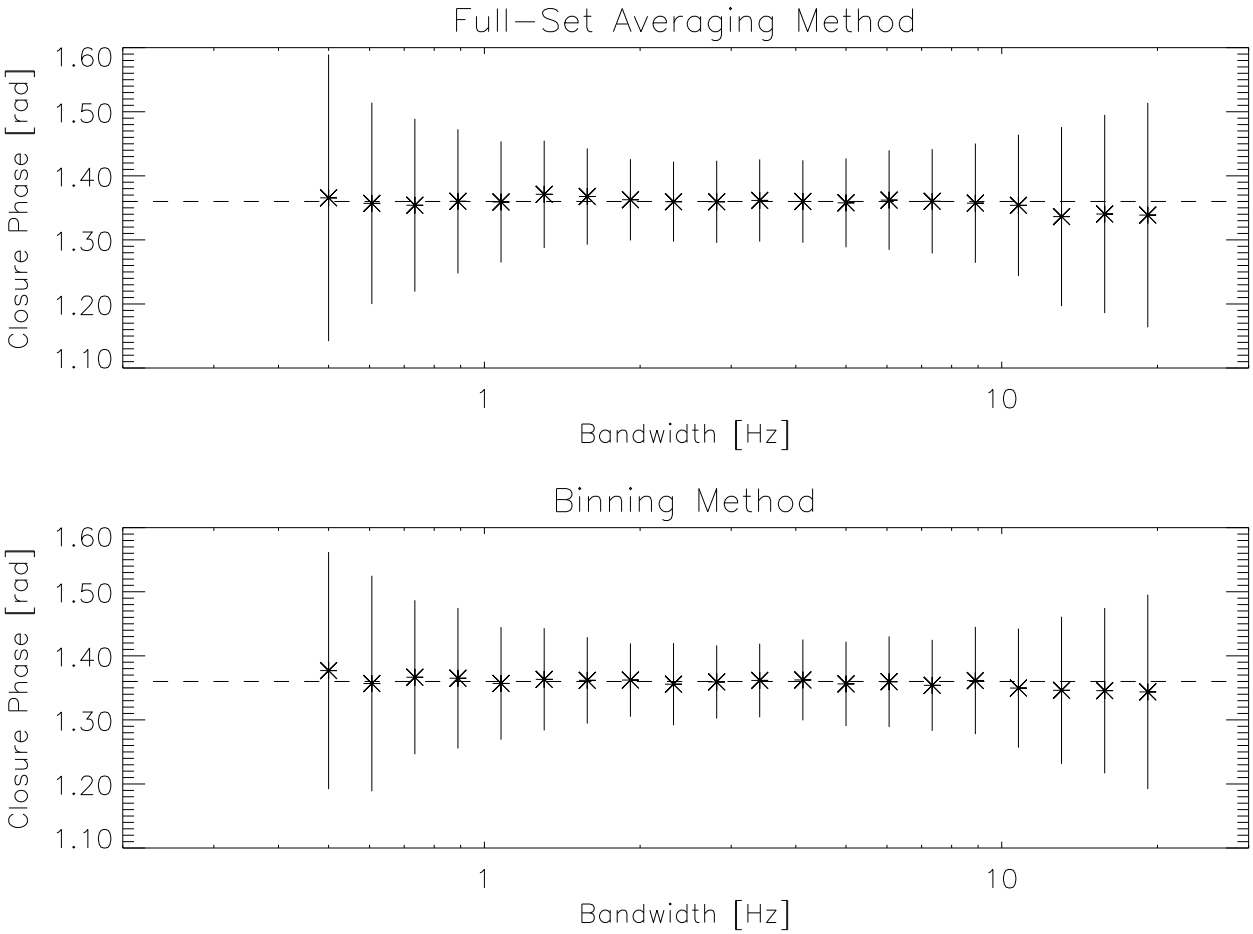

Figure 3. Closure phase calculation of simulated fringes, as a function of fringe bandwidth. The input closure phase was 1.36 as indicated by the broken horizontal line. The error bars represent the standard deviation of the mean for 100 calculations within each bandwidth measured. The top panel used the full-set averaging method, while the bottom panel used the binned Hanning window method. The quality of input fringe was of that shown in figure 2.

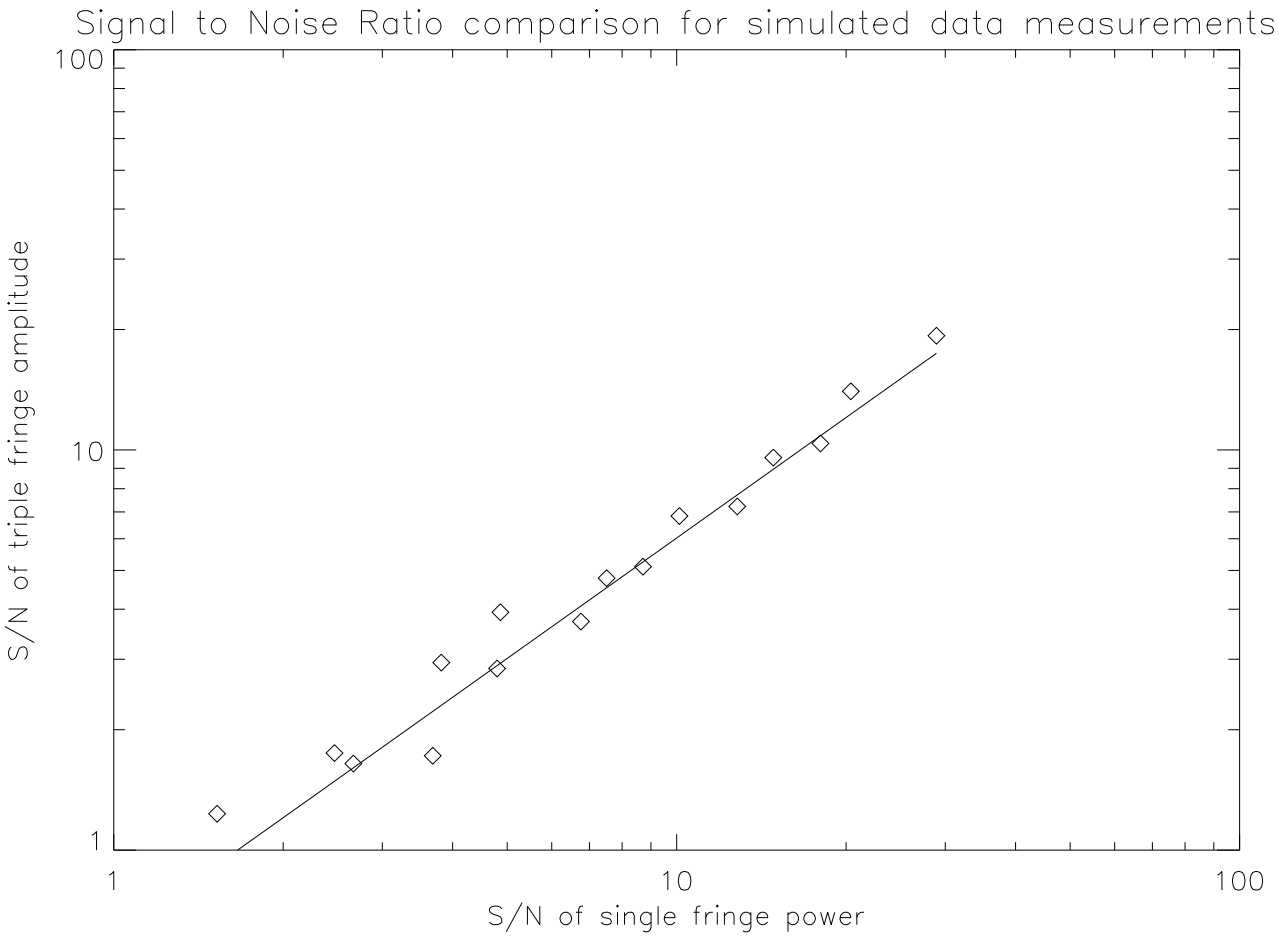

Figure 4. Measured signal to noise in a single fringe versus that in the triple product, for $(S/N)_{t_c} \ll 1$. The individual points represent measurements of a single simulated data set, using increased integration time to improve overall S/N, while the solid line represents the prediction given by equation (11b).